Supporting Information

The Efficient Strategy for Improving the Luminescent Sensing Performance of Terbium(III) Metal-Organic Framework Towards Multiple Substances

Xiaoning Wang,[1] *Jia-Luo Li,*[2] *Chenggang Jiang,*[1] *Peng Hu,*[1] *Bao Li,*[*,1] *Tianle Zhang*[1] *and Hong-Cai Zhou*[*,2,3]

[1] Key laboratory of Material Chemistry for Energy Conversion and Storage, School of Chemistry and Chemical Engineering, Huazhong University of Science and Technology, Wuhan, Hubei, 430074, P. R. China.

[2] Department of Chemistry, Texas A&M University, College Station, Texas 77843-3255, United States.

[3] Department of Materials Science and Engineering, Texas A&M University, College Station, Texas 77842, United States.

* Corresponding Author

*E-mail: libao@hust.edu.cn (B. L.).

*E-mail: zhou@chem.tamu.edu (H.-C. Z.).

Experimental Section

Materials and general methods

The organic ligand H_2L (Scheme S1-4) was synthesized according to the literature method[1] and all of the starting reagents for the syntheses were commercially available and were used as received. Elemental analyses (C, H and N) were performed on a Perkin-Elmer 2400 analyzer. The IR spectra were recorded with KBr pellets on a Nicolet Avatar-360 spectrometer in the 4000–400 cm^{-1} region. Thermogravimetric analysis (TGA) was carried out with a Perkin-Elmer TG-7 analyzer heated from room temperature to 800 °C, using a heating rate of 10 ℃ min^{-1} under air. Powder X-ray diffraction (PXRD) patterns were measured on the Rigaku model Ultima IV diffractometer with Cu-Ka radiation. The fluorescence spectra were conducted with a FLS920 spectrophotometer at room temperature. Ultraviolet-visible (UV-vis) adsorption spectra were recorded at room temperature on UV-2550 spectrophotometer.

Synthesis of 4-{bis(4-benzoic)amino}-4H-1,2,4-triazole (H_2L)

The ligand H_2L was prepared using a modified literature procedure:

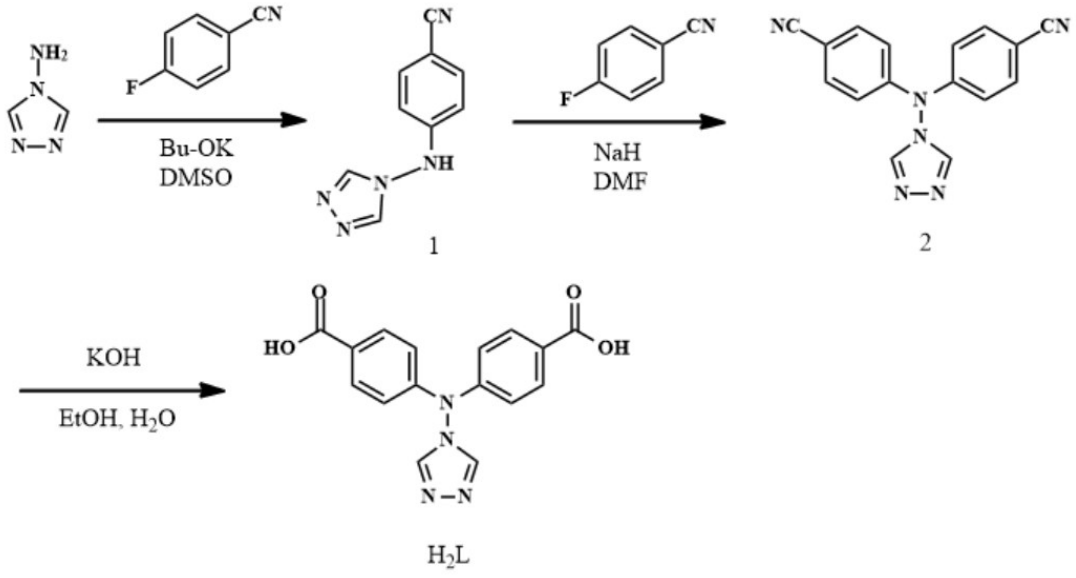

Scheme S1. Synthetic route for the organic ligand H_2L.

4-((4-cyanophenyl)amino)-4H-1,2,4-triazole (1).

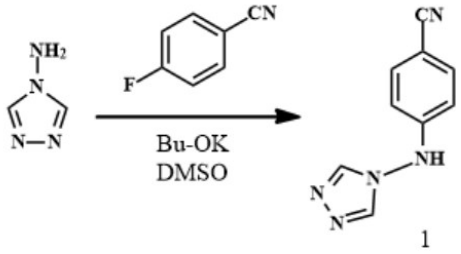

Scheme S2. Synthetic route for the organic compound 1.

4-amino-4H-1,2,4-triazole (3.36 g, 40 mmol), potassium tert-butoxide (4.48 g, 40 mmol), Dimethyl sulfoxide (DMSO) (30 mL) and a magnetic stir bar were added to a 100-mL three-neck flask under N_2 atmosphere. After stirring at room temperature for 2 h, a solution of 4-fluorobenzonitrile (2.44 g, 20 mmol) in DMSO (10 mL) was added dropwise to the reaction mixture with ice bath. The mixture was further stirred for 1.5 h at room temperature, then poured into water, and neutralized with 1 M hydrochloric acid (HCl) to pH = 7. The precipitate that formed was filtered and purified by recrystallizing from water to obtain the white solid (2.4 g, yield: 64.9%): ^{1}H-NMR (DMSO-d_6): δ: 6.57 (2H, d, J = 9 Hz), 7.69 (2H, d, J = 9 Hz), 8.83 (2H, s).

4-{bis(4-cyanophenyl)amino}-4H-1,2,4-triazole (2)

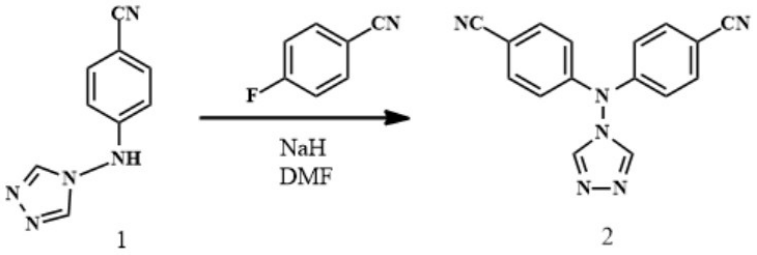

Scheme S3. Synthetic route for the organic compound 2.

4-((4-cyanophenyl)amino)-4H-1,2,4-triazole (1) (2.4 g, 13mmol) was added sodium hydride (0.48 g) in N,N-dimethylformamide (DMF) (40 mL) with ice bath under N_2 atmosphere. Then the mixture was stirred for 30 min at 40–50 °C, and cooled to room temperature. 4-Fluorobenzonitrile (1.6 g, 0.026 mmol) was added and the reaction mixture was stirred for 2 h at 80 °C. After the reaction mixture was allowed to cool to room temperature, water (400 mL) was added to the resultant residue and the whole solution was extracted with $CHCl_3$, the organic layer was washed with water, dried over Na_2SO_4 and then over vacuum. The yellow liquid was obtained and poured into

water (200mL) and stirred vigorously. The formed precipitate was collected by filtration and dried under reduced pressure at 80 °C overnight to afford white solid 4-{bis(4-cyanophenyl)amino}-4H-1,2,4-triazole (1.8 g, yield: 48.6%). ^{1}H-NMR (DMSO-d_6): δ: 7.04 (4H, d, J = 9 Hz), 7.69 (4H, d, J = 9 Hz) 8.44 (2H, s).

4-{bis(4-benzoic)amino}-4H-1,2,4-triazole (H_2L)

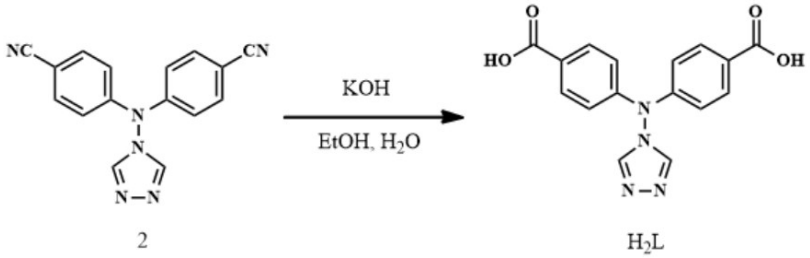

Scheme S4. Synthetic route for the organic ligand H_2L.

4-{bis(4-cyanophenyl)amino}-4H-1,2,4-triazole (2) (1.6 g, 5.6mmol), potassium hydroxide (4.7 g, 84mmol), H_2O (30 ml) and ethanol (EtOH) (30 ml) were added to a 150-mL one-neck flask equipped with a condenser and a magnetic stirrer. Then the reaction mixture was heated at 110 °C for 24 h. After the reaction mixture was allowed to cool to room temperature, EtOH was removed from the solution. Then water (150 ml) was added and the resulting solution was filtered. The clear filtrate was acidified with 2M hydrochloric acid (HCl) until its pH reach 3～4. The precipitate that formed was collected by filtration, and recrystallized and dried under reduced pressure at 80 °C for 24 h to obtain the final white solid product (1.35 g, yield: 75%). ^{1}H-NMR (400 MHz, DMSO-d6) δ: 12.96 (s, 2H), 9.23 (s, 2H), 7.97 (d, J = 8.4 Hz, 4H), 7.07 (d, J = 8.8 Hz, 4H).

Synthesis of 1

A mixture of $Tb(NO_3)_3 \cdot 6H_2O$ (0.046 g, 0.1 mmol), H_2L (0.026 g, 0.05 mmol), 3-AT (0.042 g, 0.5 mmol), DMA (3 mL), and H_2O (2 mL) was sealed in a Teflon-lined stainless steel vessel, which was heated at 80 °C for 48 h in an oven. After cooling to room temperature, colorless prism single crystals were obtained. The yield was 60% for **1** (based on H_2L ligand). Elemental analysis calcd (%) for **1** ($C_{96}H_{82}N_{24}O_{32}Tb_4$): C, 42.40; H, 3.04; N, 12.36; found: C, 42.53, H, 3.09, N, 12.46.

Single crystal X-ray diffraction

The crystal data for **1** were collected on BL17B at the Shanghai Synchrotron Radiation Facility (Shanghai, China) and processed with HKL3000. The structure of the **1** was solved by direct methods, and the non-hydrogen atoms were located from the trial structure and then refined anisotropically with SHELXTL using a full-matrix least squares procedure based on F^2 values.[2] All hydrogen atoms were generated geometrically and refined using a riding model. The contribution of the missing solvent molecule and other ionic residues to the diffraction patterns was removed from the reflection data by the SQUEEZE method as implemented in PLATON to afford a set of solvent free diffraction intensities.[3] The details for structural analyses of the **1** were listed in Table S1 and Table S2.

The related formula used in description of luminescent sensing

Quenching efficiency = $(I_0 - I)/I_0 \times 100\%$, where the I_0 and I are the luminescent intensities of the $^5D_4 \rightarrow {}^7F_5$ of Tb^{3+} ion at 543 nm before and after addition of the targeted species.

The luminescent quenching efficiency was quantitatively calculated using the Stern−Volmer (S−V) equation: $I_0/I = K_{SV}[M] + 1$, where the I_0 and I are the maximum luminescent intensities before and after the addition of Fe^{3+} ion, [M] is the molar concentration of Fe^{3+} ion, and K_{SV} is the quenching constant (M^{-1}).

The structure of 1

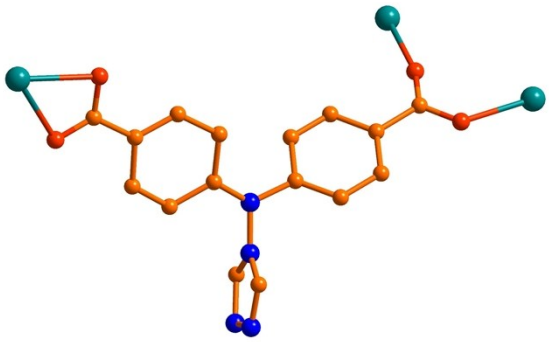

Figure S1. The coordination modes of H_2L ligand in **1**.

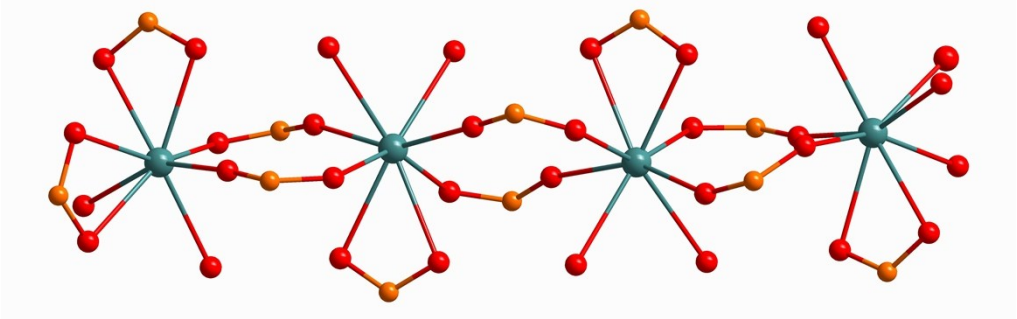

(a)

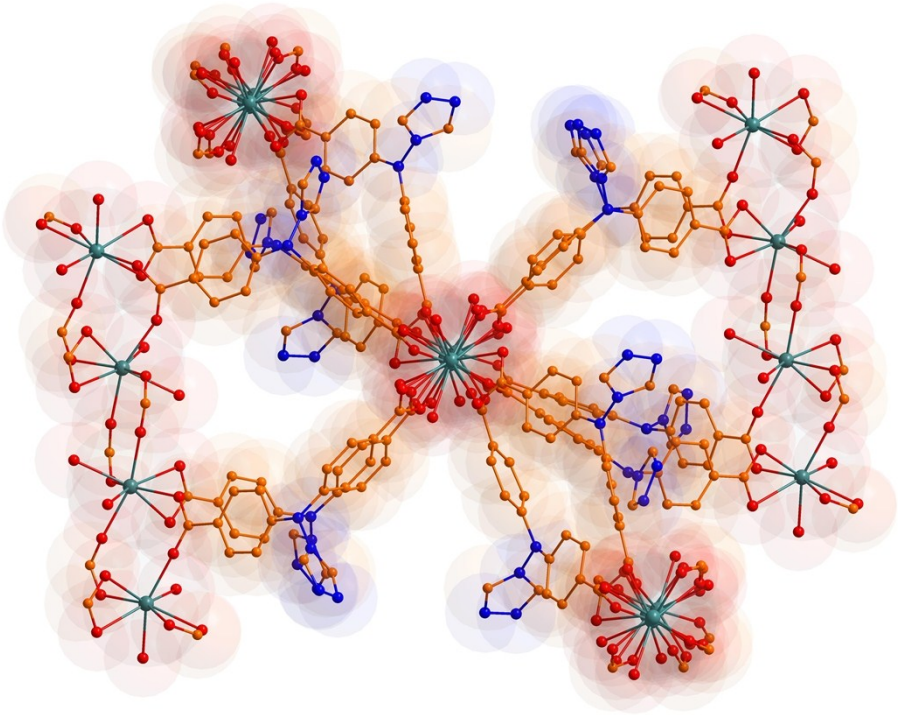

(b)

Figure S2. The Tb_4 cluster (a) and connection mode of adjacent Tb_4 clusters (b) of **1**.

Table S1. Crystal data and structure refinement details for **1**.

1	
formula	$C_{96}\ H_{82}\ N_{24}\ O_{32}\ Tb_4$
formula weight	2719.53
crystal system	Monoclinic
space group	$P2_1/c$
a (Å)	18.886(4)

b (Å)	32.064(6)
c (Å)	25.879(5)
α (deg)	90
β (deg)	104.04(3)
γ (deg)	90
Z	4
V (Å3)	15203(6)
μ(Mo/Cu Kα) (mm^{-1})	1.901
F(000)	5368.0
temperature (K)	293(2)
theta min, max(deg)	2.222, 61.554
$^{a}R_1$, ^{b}wR [$I \geq 2\sigma(I)$]	0.1148, 0.2914
GOF on F^2	1.087
R_1, wR_2 (all data)	0.1158, 0.2919
Reflns completeness	99.40
$^{a}R_1=\Sigma\|\|F_o\|-\|F_c\|\|/\|\Sigma\|F_o\|$. $wR_2=\{\Sigma[w(F_o^2-F_c^2)^2]/\Sigma[w(F_o^2)^2]\}^{1/2}$; $w=1/[\sigma^2(F_o^2)+(aP)^2+bP]$ and $P=(F_o^2+2F_c^2)/3$.	

Table S2. Selected Bond Distances for **1**.

Atom	Atom	Length/Å	Atom	Atom	Length/Å
Tb1	O8[1]	2.506(5)	C15	C14	1.336(8)
Tb1	O7[1]	2.417(6)	C15	C01C	1.516(8)
Tb1	O5	2.253(6)	C33	C34	1.389(8)
Tb1	O26	2.353(6)	O21	Tb4[4]	2.428(6)
Tb1	O4	2.404(6)	O24	Tb3	2.363(5)
Tb1	O25	2.352(7)	O19	Tb4[1]	2.390(6)
Tb1	O14	2.278(6)	O15	Tb4[1]	2.355(6)
Tb1	O3	2.404(6)	O16	Tb3[1]	2.296(6)
Tb1	C24[1]	2.813(7)	O11	Tb3[3]	2.489(6)
Tb1	C8	2.745(8)	O12	Tb3[3]	2.456(7)
Tb2	O27	2.501(6)	O2	Tb2[4]	2.324(6)
Tb2	O10	2.447(6)	O1	Tb3[4]	2.256(7)
Tb2	O6	2.401(6)	C33	Tb3[3]	2.844(9)
Tb2	O13	2.289(6	C72	Tb4[1]	2.801(7)
Tb2	O9	2.467(6)	C24	Tb1[3]	2.813(7)

Tb2	O23	2.275(6)	C88	Tb4[4]	2.776(7)
Tb2	O28	2.466(6)	O22	Tb4[4]	2.408(6)
Tb2	O2[2]	2.324(6)	Tb3	O16[3]	2.296(6)
Tb2	C40	2.828(8)	Tb3	O11[1]	2.489(6)
Tb4	O20[3]	2.477(5)	Tb3	O12[1]	2.456(7)
Tb4	O21[2]	2.428(6)	Tb3	O1[2]	2.256(7)
Tb4	O19[3]	1.211(7)	Tb3	C33[1]	2.844(9)
Tb4	O15[3]	1.368(7)	O20	Tb4[1]	1.382(7)
Tb4	O18	1.410(7)	O20	C72	1.283(10)
Tb4	O31	1.458(7)	O8	Tb1[3]	2.506(5)
Tb4	O32	1.235(7)	O8	C24	1.266(8)
Tb4	C72[3]	1.260(7)	O7	Tb1[3]	2.417(6)
Tb4	C88[2]	1.410(7)	O7	C24	1.258(9)
Tb4	O22[2]	1.192(8)			

Symmetry code for **1**: [1]+X,1/2-Y,-1/2+Z; [2]1+X,+Y,+Z; [3]+X,1/2-Y,1/2+Z; [4]-1+X,+Y,+Z.

Table S3. The vapor pressure parameter of the targeted NACs.[4-7]

Targeted NACs	**Vapor Pressure (in mmHg, at 25 °C)**	**Reduction Potential (in V vs SCE)**
Nitrobenzene (NB)	0.2416	−1.15
2-Nitrotoluene (2-NT)	0.1602	−1.2
2,4-Dinitrotoluene (2, 4-DNT)	1.44×10^{-6}	−1.0
1,3-dinitrobenzene (1, 3-DNB)	8.82×10^{-4}	−0.9
1,4-Dinitrobenzene (1,4-DNB)	2.406×10^{-5}	−0.7
2,4,6-trinitrophenol (TNP)	5.81×10^{-9}	−0.63

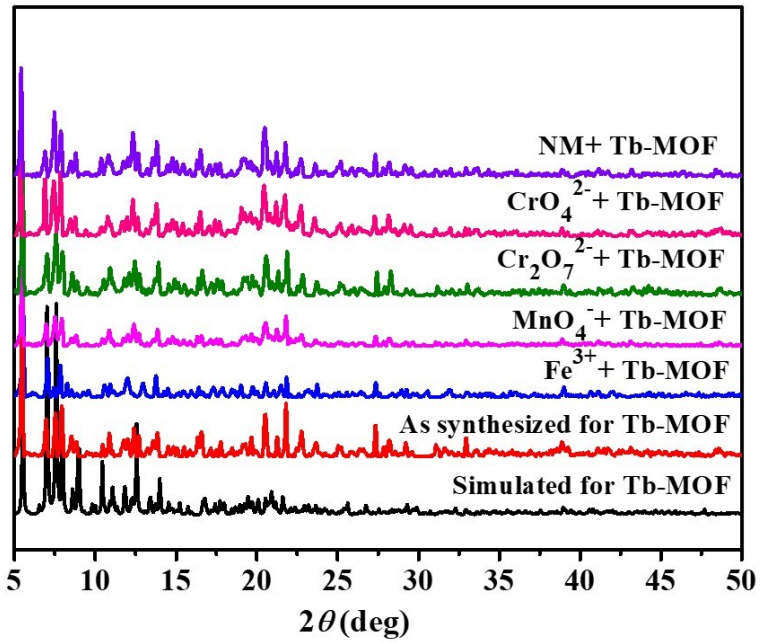

Figure S3. PXRD patterns of **1** and samples after immersing in Fe^{3+}, MnO_4^-, $Cr_2O_7^{2-}$, CrO_4^{2-} as well as NM aqueous solutions.

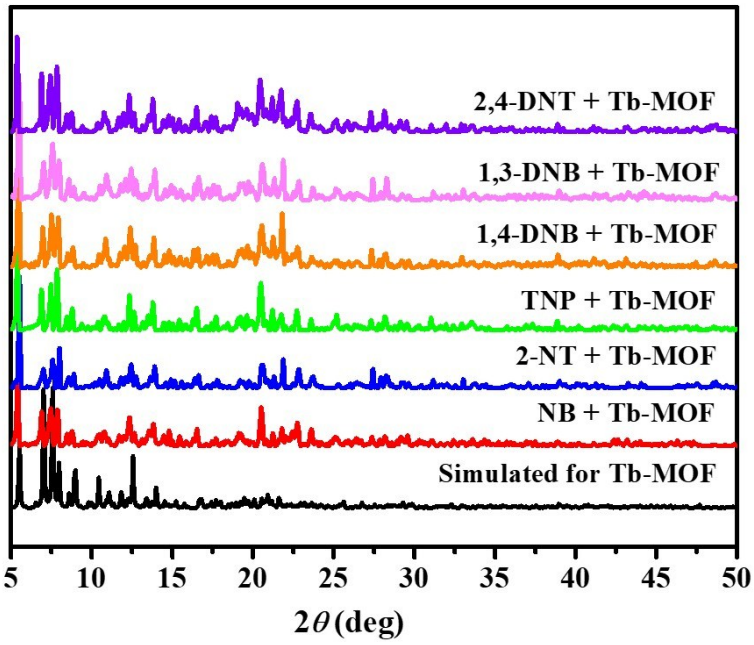

Figure S4. PXRD patterns of **1** after immersing in targeted NACs.

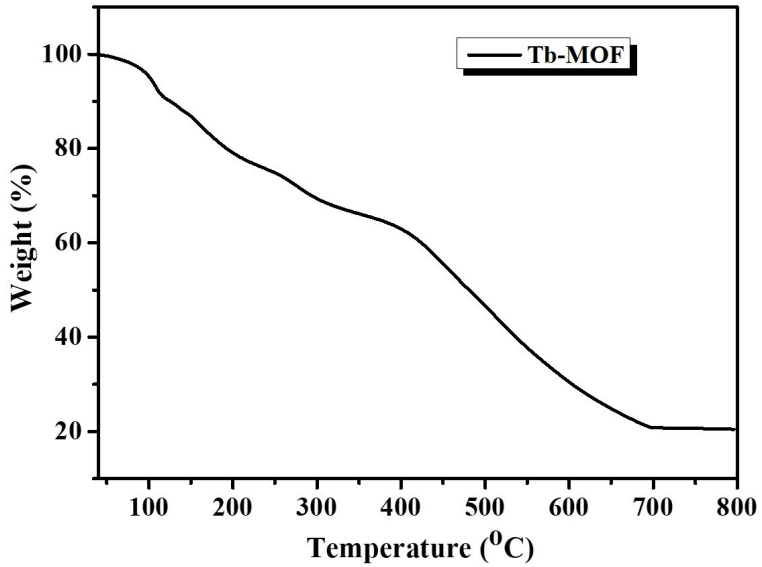

Figure S5. TGA curves of **1** under air atmosphere.

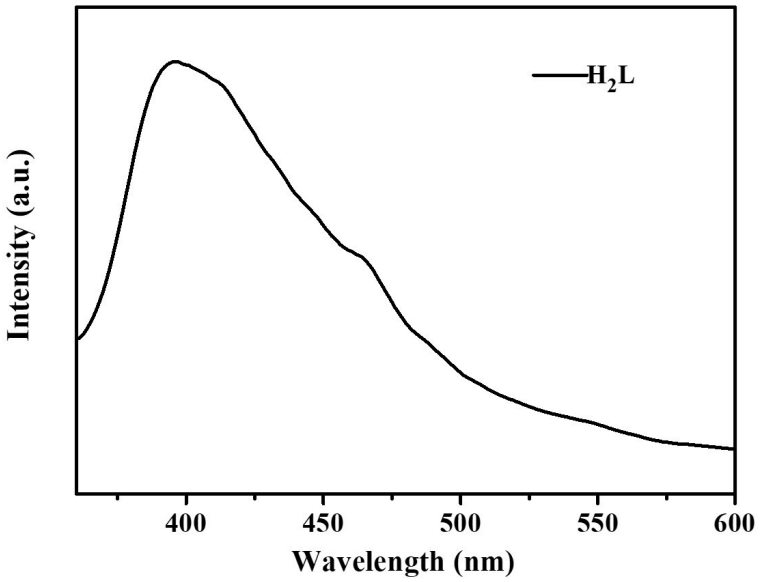

(a)

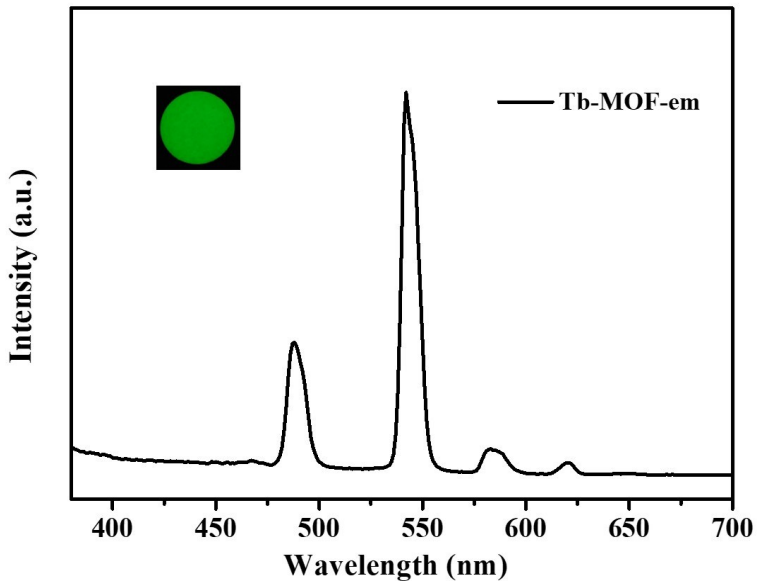

(b)

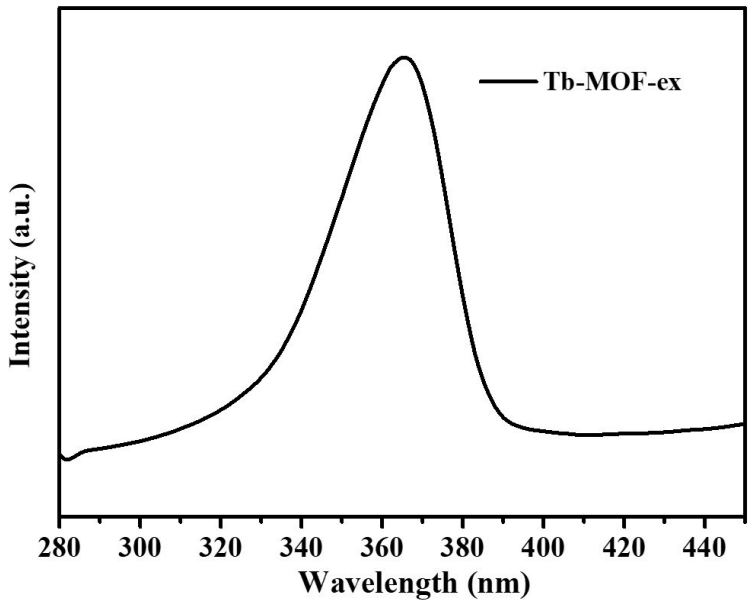

(c)

Figure S6. Solid-state luminescent spectra of H_2L (a), **1** (b) and the excitation spectra of **1** (c). The free H_2L ligand exhibits a broad emission band at 396 nm (λ_{ex} = 360 nm), which is probably derived from the ligand-based $\pi^* \rightarrow \pi$ transitions.

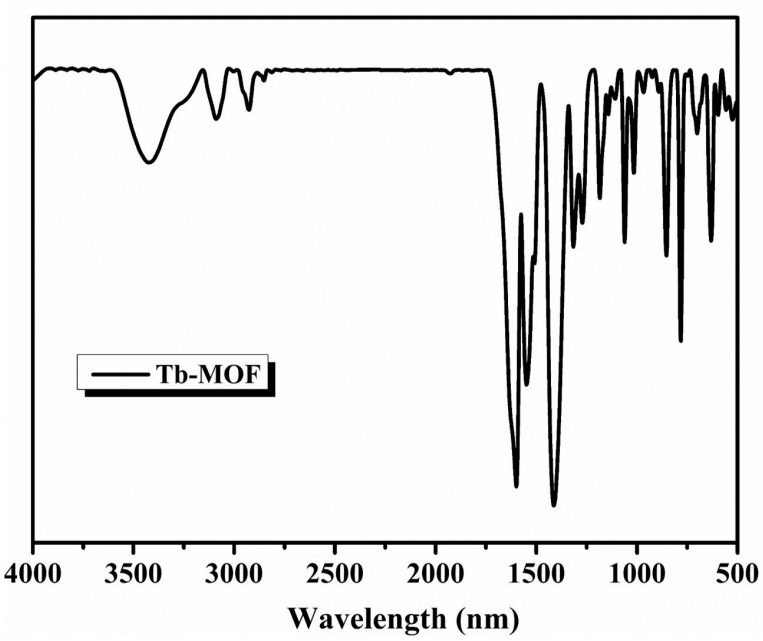

Figure S7. IR spectra of **1**.

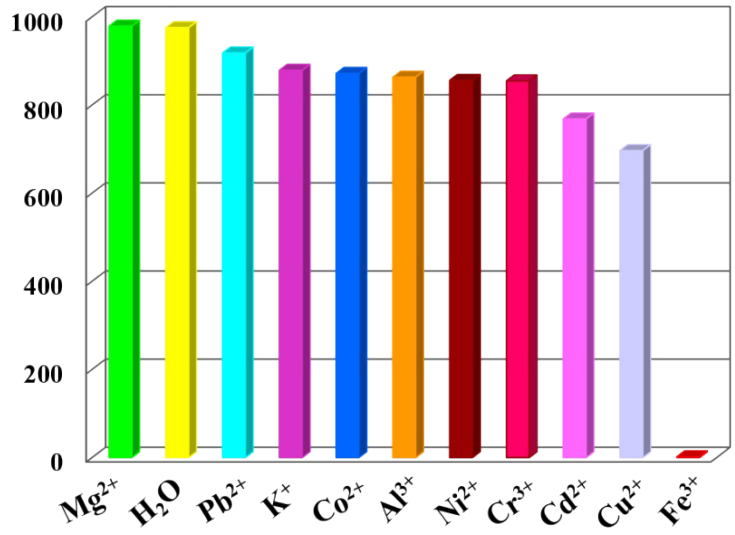

Figure S8. Luminescence emission intensities of $^5D_4$-$^7F_5$ transitions of **1** immersed into aqueous solution of various cations.

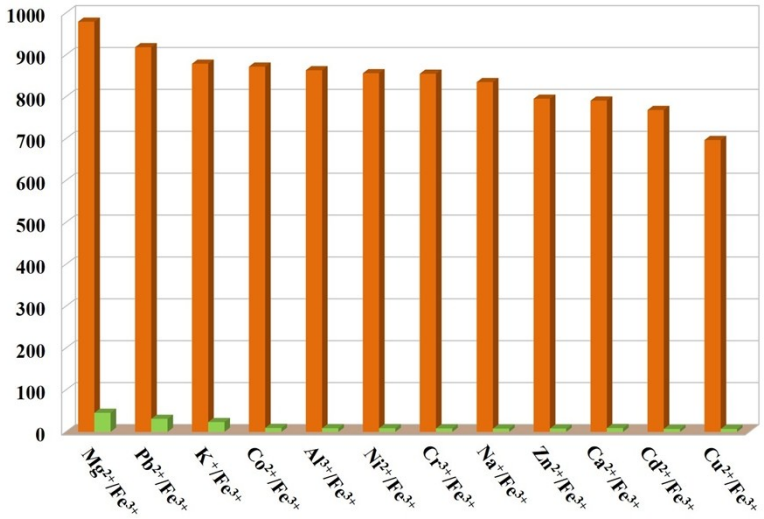

Figure S9. The competition experiments for the detection of Fe^{3+} ion in the presence of the interference metal cations.

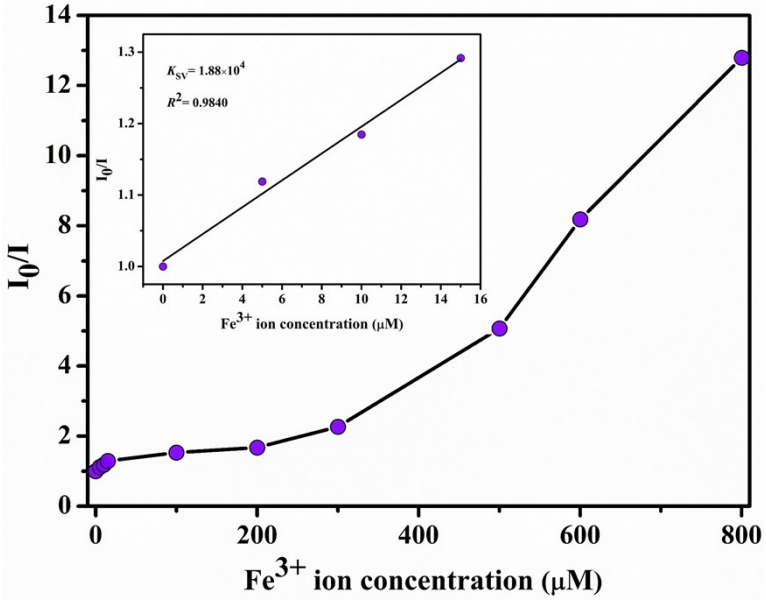

Figure S10. SV curve for **1** by gradual addition of Fe^{3+}. The inset demonstrates the quenching relationship at low concentrations of Fe^{3+}.

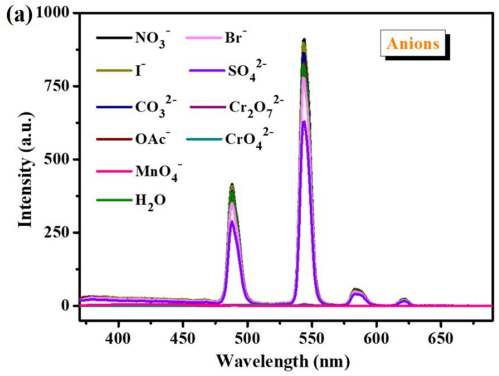
(a)
Anions
NO3-
Br-
I-
SO4 2-
CO3 2-
Cr2O7 2-
OAc-
CrO4 2-
MnO4-
H2O
Intensity (a.u.)
Wavelength (nm)

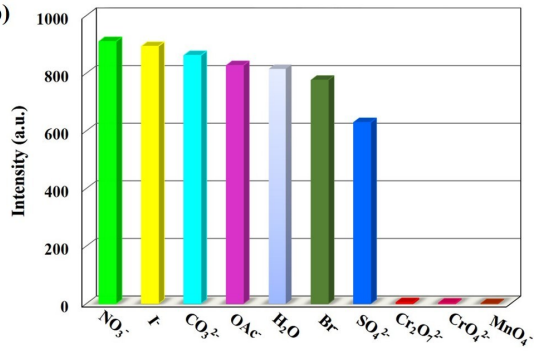
(b)
Intensity (a.u.)
NO3-
I-
CO3 2-
OAc-
H2O
Br-
SO4 2-
Cr2O7 2-
CrO4 2-
MnO4-

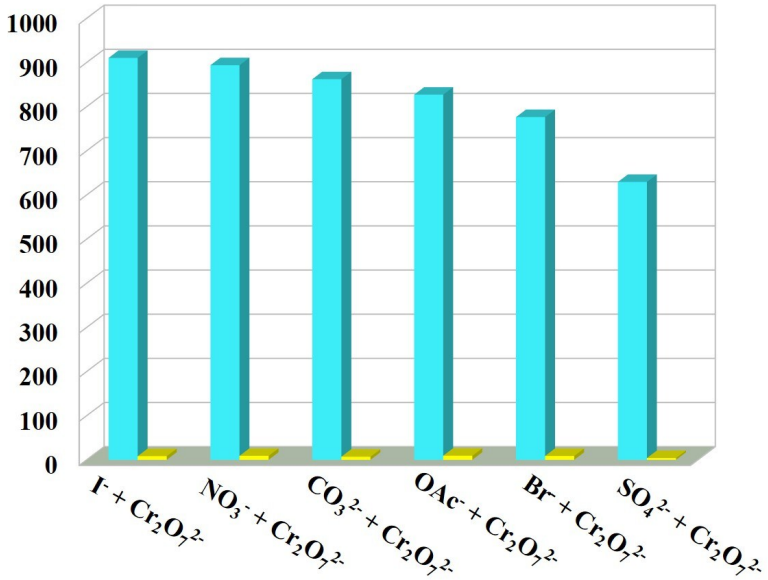
I- + Cr2O7 2-
NO3- + Cr2O7 2-
CO3 2- + Cr2O7 2-
OAc- + Cr2O7 2-
Br- + Cr2O7 2-
SO4 2- + Cr2O7 2-

(c)

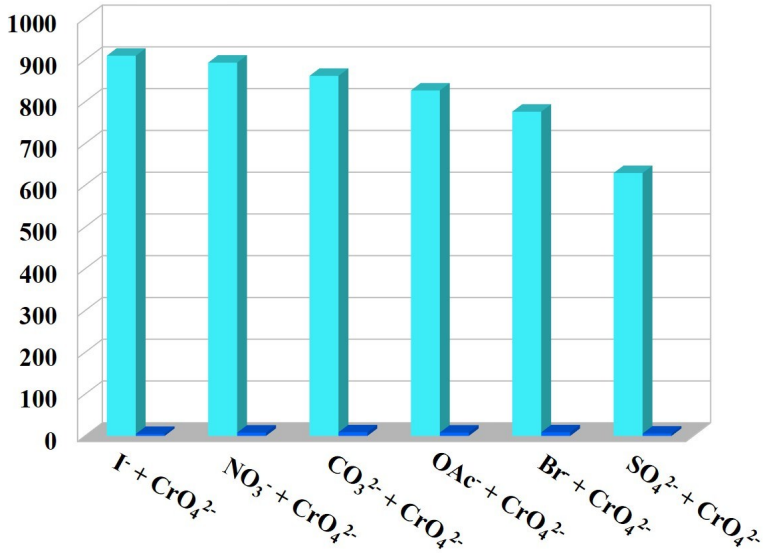
I- + CrO4 2-
NO3- + CrO4 2-
CO3 2- + CrO4 2-
OAc- + CrO4 2-
Br- + CrO4 2-
SO4 2- + CrO4 2-

(d)

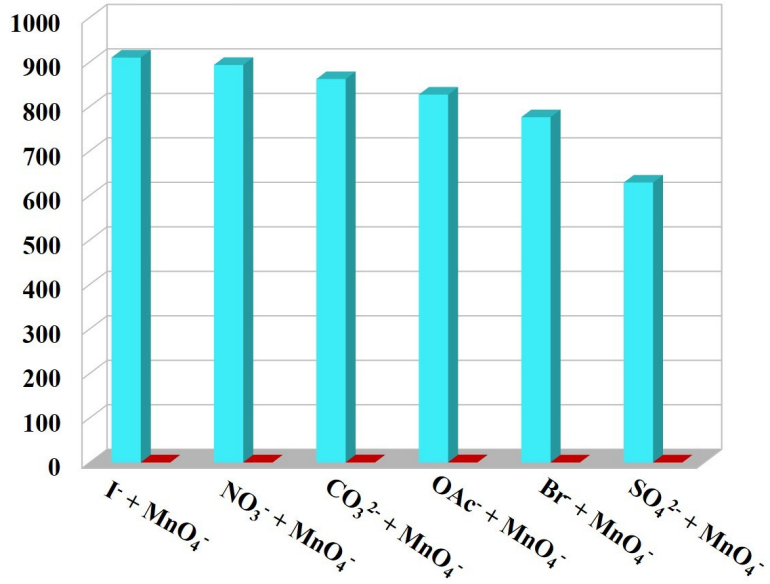

(e)

Figure S11. Luminescence spectra (a) and Luminescence intensities of the $^5D_4$-$^7F_5$ transitions (b) of **1** immersed into aqueous solution containing various anions.The competition experiments for the detection of CrO_4^{2-} (c), $Cr_2O_7^{2-}$ (d) and MnO_4^- anions (e) in the presence of the interference anions.

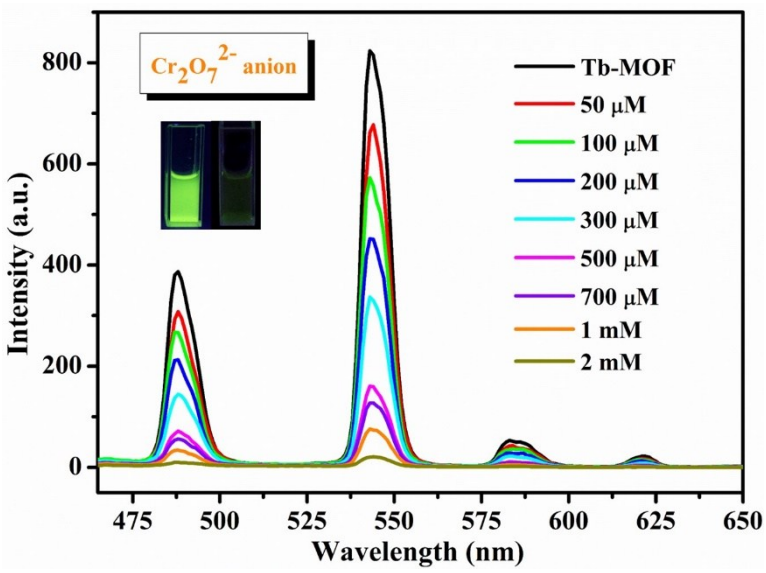

(a)

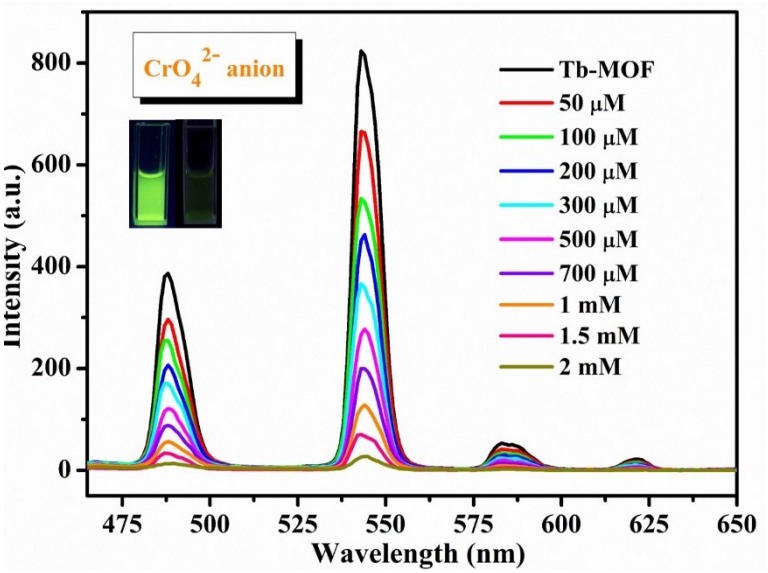

(b)

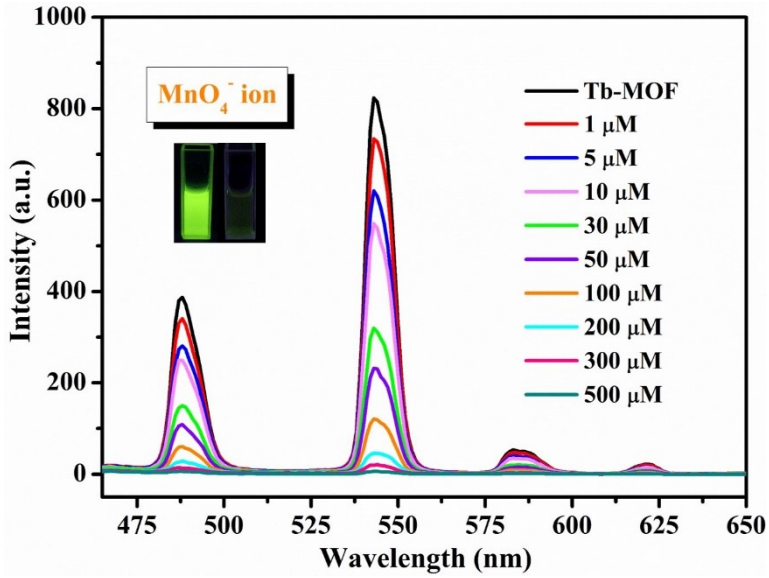

(c)

Figure S12. Luminescence emission spectra of **1** in aqueous solutions containing different concentrations of $Cr_2O_7^{2-}$ (a), CrO_4^{2-} (b) and MnO_4^- (c) ions.

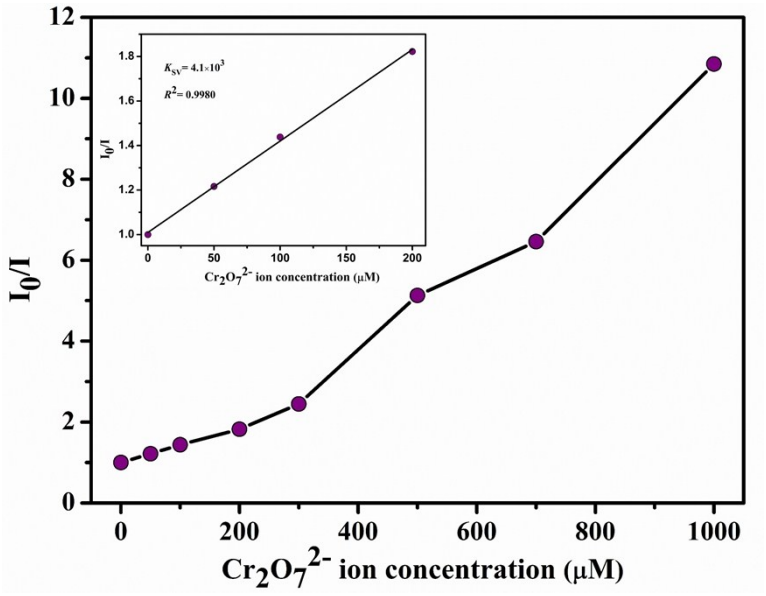
K_{SV}= 4.1×10^3
R^2= 0.9980
I_0/I
$Cr_2O_7^{2-}$ ion concentration (μM)
I_0/I
$Cr_2O_7^{2-}$ ion concentration (μM)

(a)

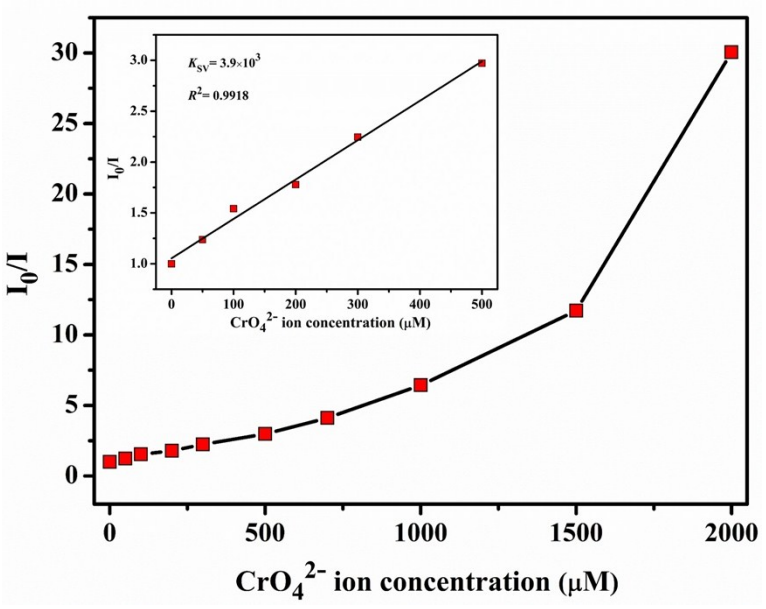
K_{SV}= 3.9×10^3
R^2= 0.9918
I_0/I
CrO_4^{2-} ion concentration (μM)
I_0/I
CrO_4^{2-} ion concentration (μM)

(b)

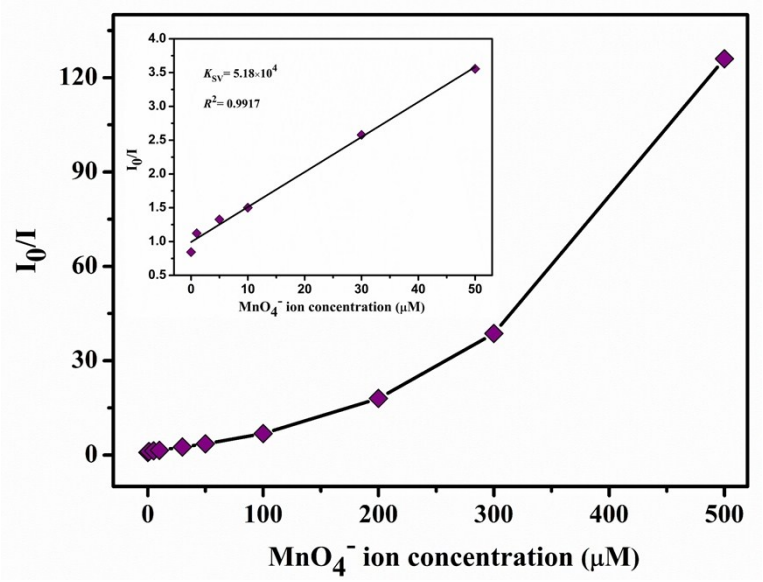

(c)

Figure S13. SV curves for **1** by gradual addition of $Cr_2O_7^{2-}$ (a), CrO_4^{2-} (b) and MnO_4^- ions (c). The inset demonstrates the quenching relationship at low concentrations of $Cr_2O_7^{2-}$, CrO_4^{2-} and MnO_4^- ions.

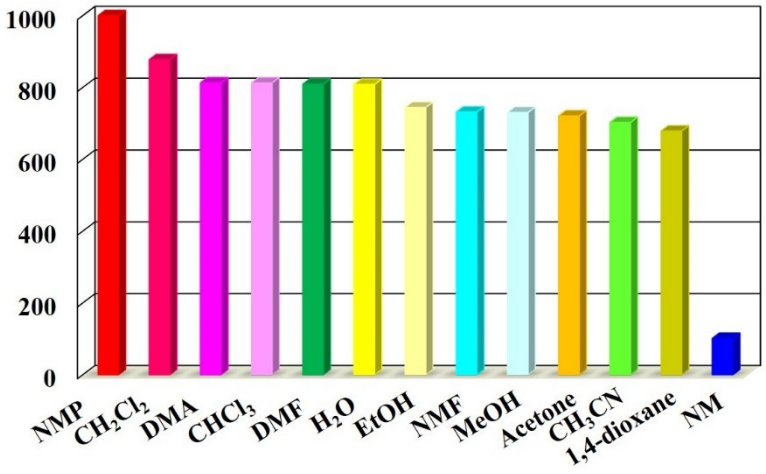

Figure S14. Luminescence emission intensities of $^5D_4$-$^7F_5$ transitions of **1** immersed into aqueous solution of various solvents.

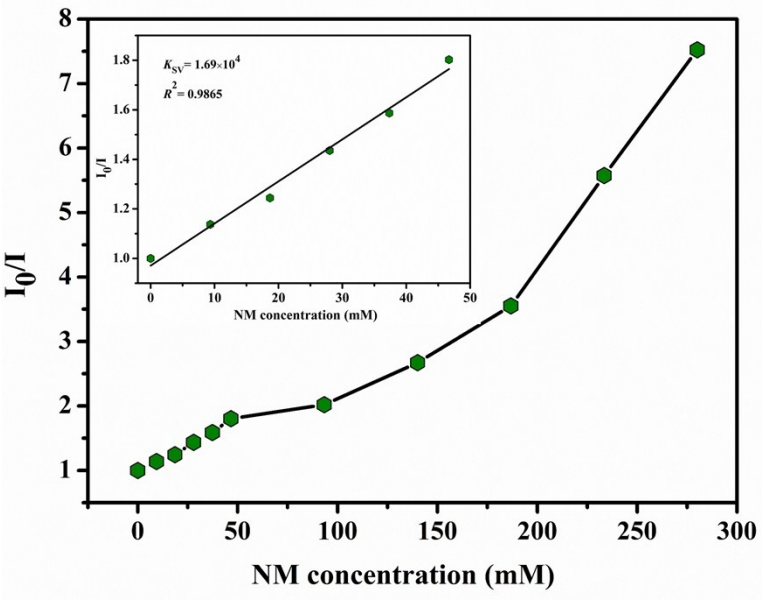

Figure S15. SV curve for **1** by gradual addition of NM. The inset demonstrates the quenching relationship at low concentrations of NM.

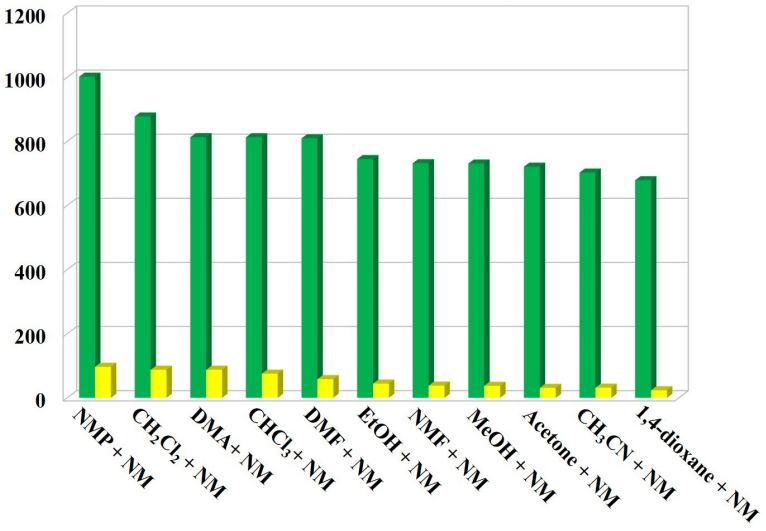

Figure S16. The competition experiments for the detection of NM in the presence of the interference organic solvents. such as N,N-dimethylformamide (DMF), N,N-dimethylacetamide (DMA), acetone, methanol (MeOH), ethanol (EtOH), dichloromethane (CH_2Cl_2), trichloromethane ($CHCl_3$), N-methyl-2-pyrrolidone (NMP), N-Methylformamide (NMF), acetonitrile (CH_3CN), 1,4-dioxane and nitromethane (NM).

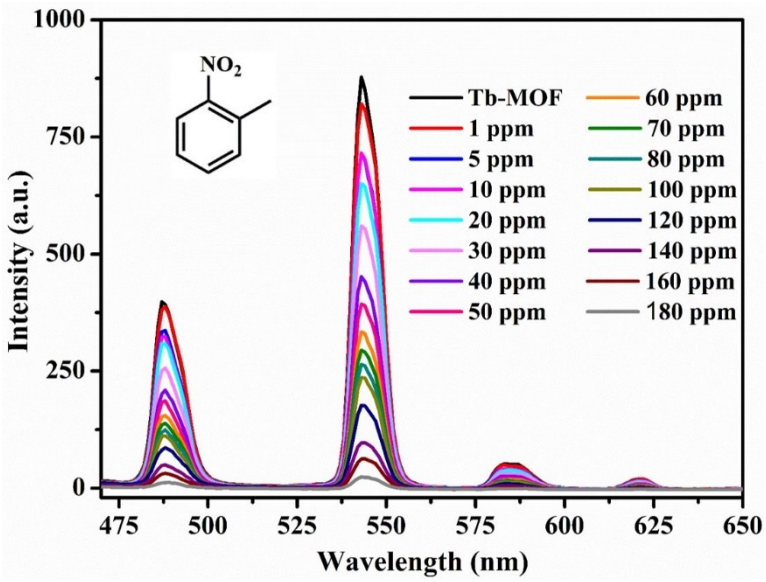
1000
750
500
250
0
Intensity (a.u.)
475
500
525
550
575
600
625
650
Wavelength (nm)
NO2
Tb-MOF
1 ppm
5 ppm
10 ppm
20 ppm
30 ppm
40 ppm
50 ppm
60 ppm
70 ppm
80 ppm
100 ppm
120 ppm
140 ppm
160 ppm
180 ppm

(a)

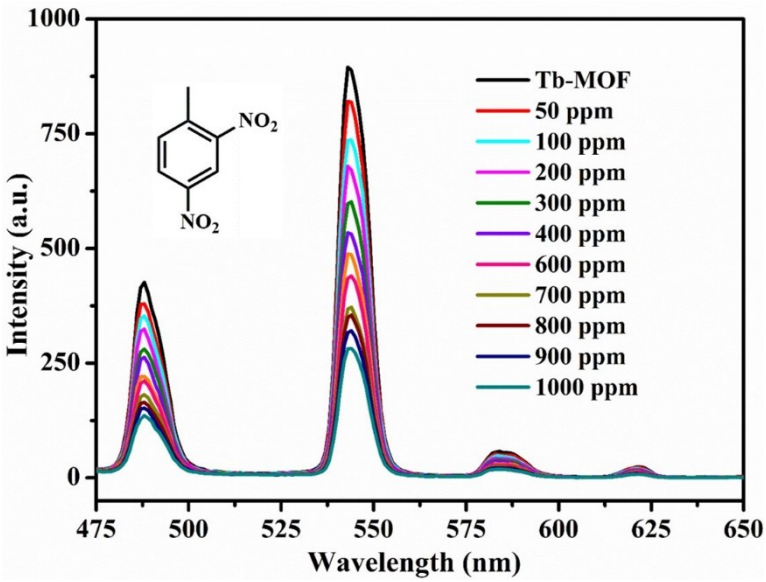
1000
750
500
250
0
Intensity (a.u.)
475
500
525
550
575
600
625
650
Wavelength (nm)
NO2
NO2
Tb-MOF
50 ppm
100 ppm
200 ppm
300 ppm
400 ppm
600 ppm
700 ppm
800 ppm
900 ppm
1000 ppm

(b)

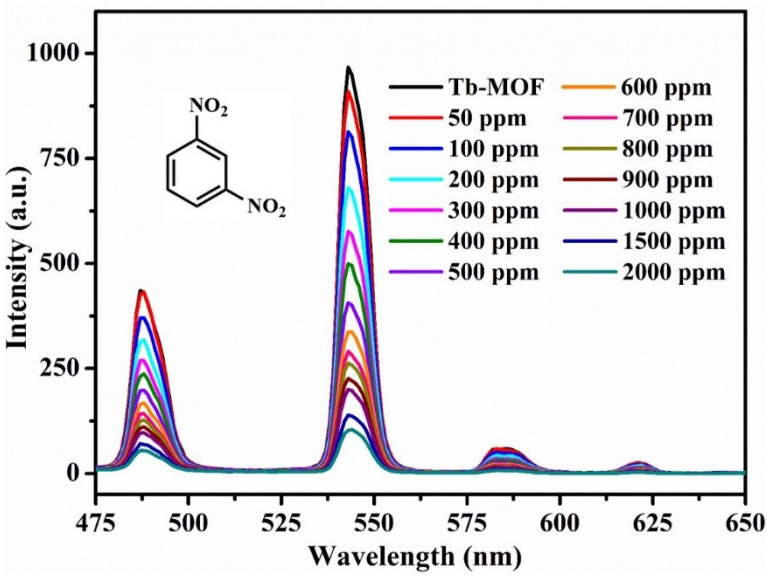

(c)

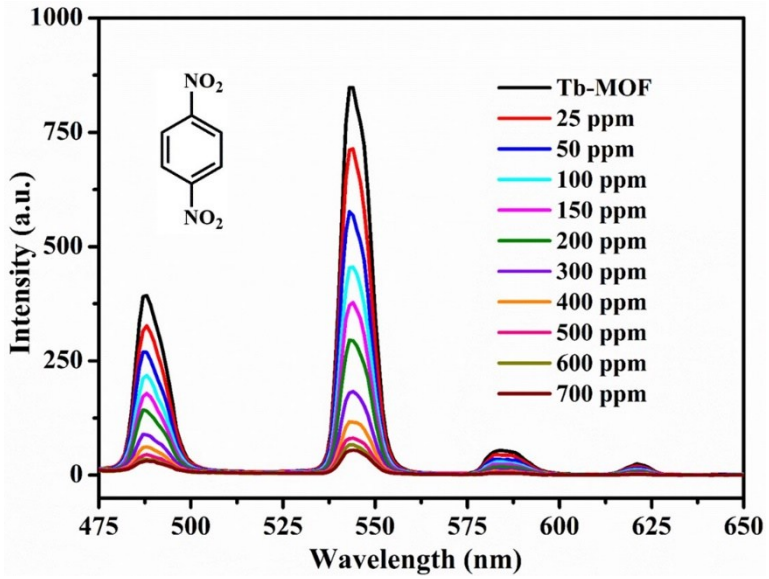

(d)

Figure S17. Fluorescence titration of **1** dispersed in aqueous solution by gradual addition of 2-NT (a) /2, 4-DNT (b) /1, 3-DNB (c) /1, 4-DNB (d).

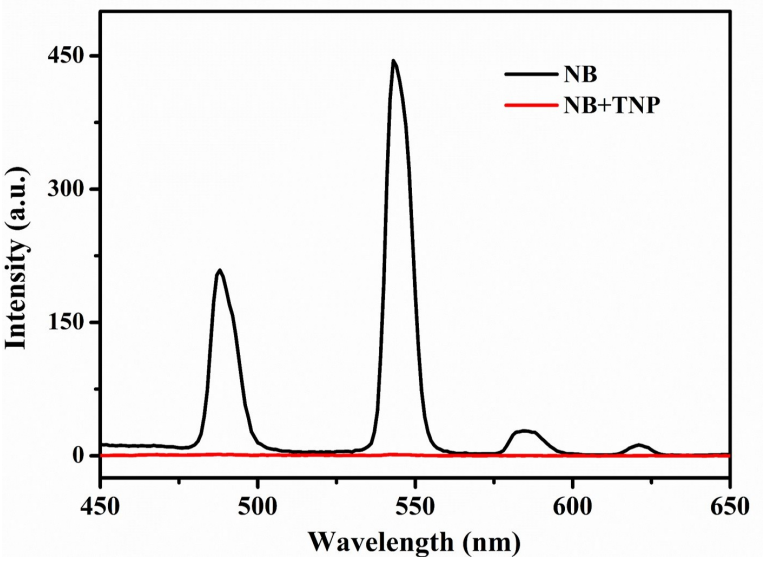
NB
NB+TNP
Intensity (a.u.)
Wavelength (nm)
0
150
300
450
500
550
600
650

(a)

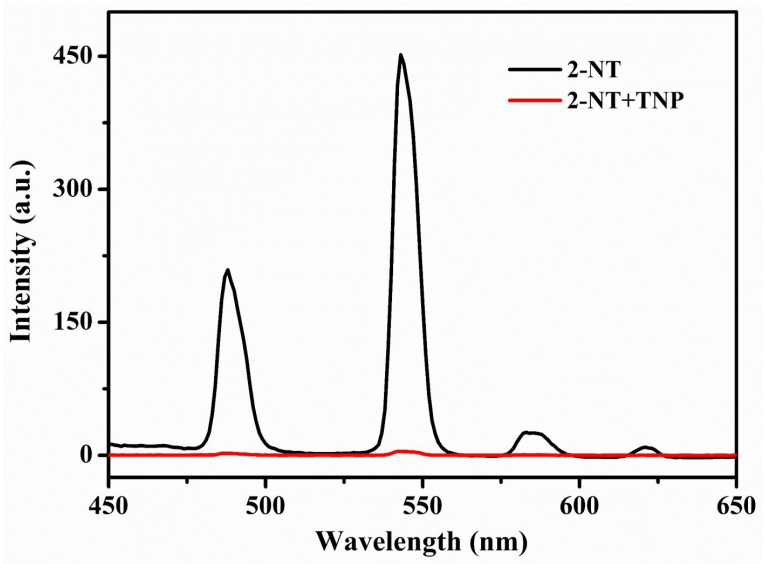
2-NT
2-NT+TNP
Intensity (a.u.)
Wavelength (nm)
0
150
300
450
500
550
600
650

(b)

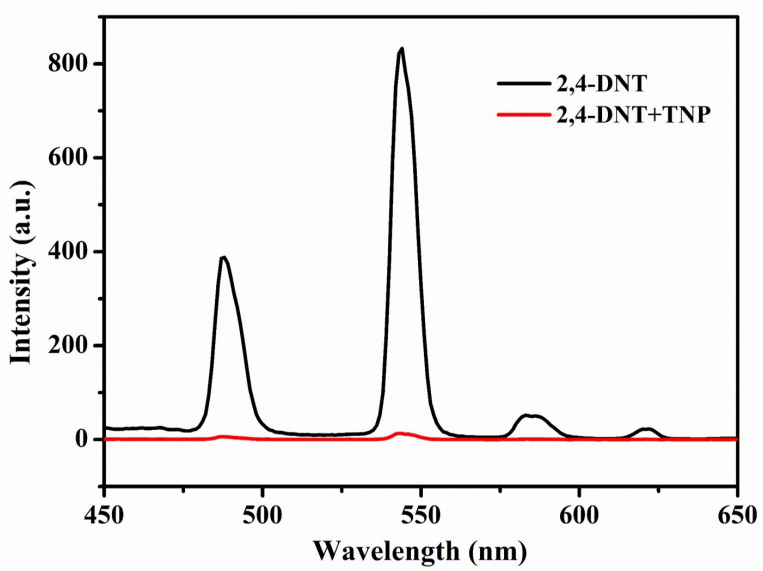
2,4-DNT
2,4-DNT+TNP
Intensity (a.u.)
Wavelength (nm)
0
200
400
600
800
450
500
550
600
650

(c)

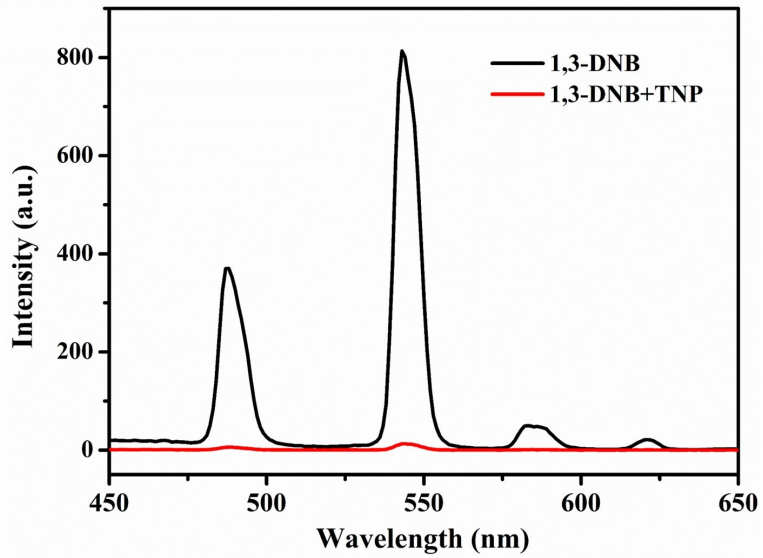
1,3-DNB
1,3-DNB+TNP
Intensity (a.u.)
Wavelength (nm)
0
200
400
600
800
450
500
550
600
650

(d)

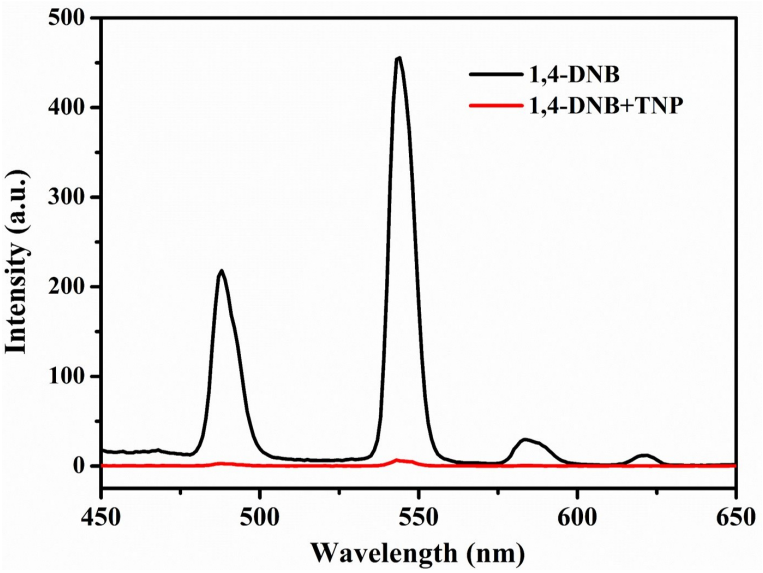

(e)

Figure S18. Emission spectra of **1** soaking in the single and mixed NACs aqueous solutions with TNP.

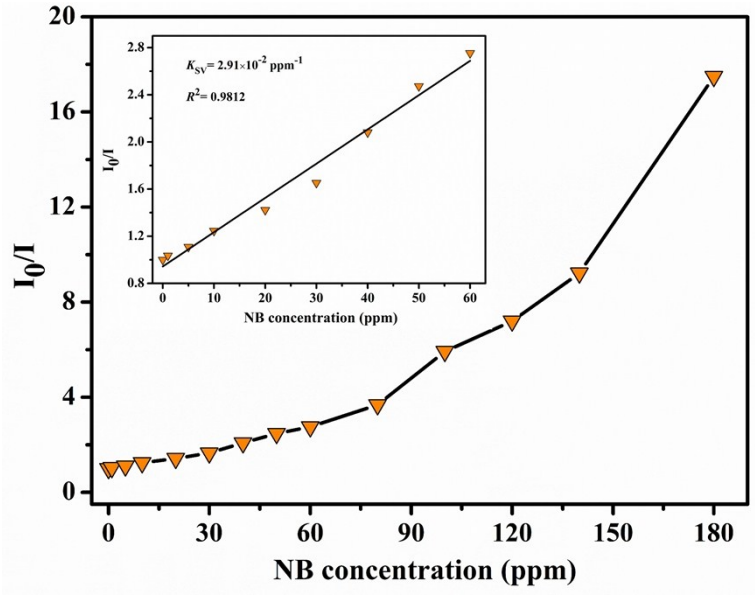

Figure S19. SV curve for **1** by gradual addition of NB. The inset demonstrates the quenching relationship at low concentrations of NB.

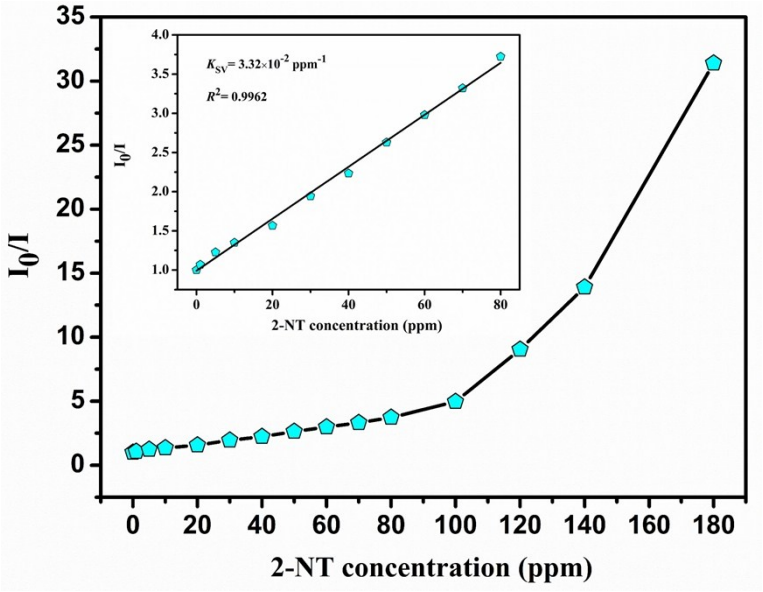

Figure S20. SV curve for **1** by gradual addition of 2-NT. The inset demonstrates the quenching relationship at low concentrations of 2-NT.

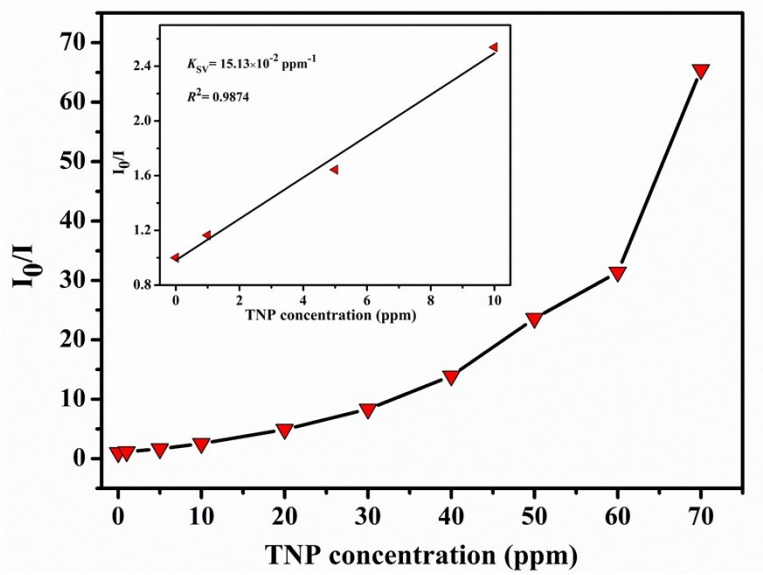

Figure S21. SV curve for **1** by gradual addition of TNP. The inset demonstrates the quenching relationship at low concentrations of TNP.

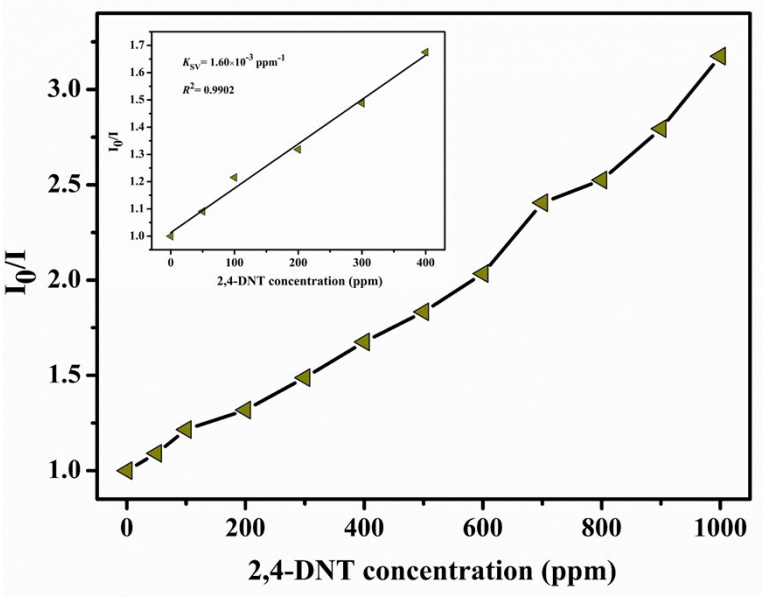

Figure S22. SV curve for **1** by gradual addition of 2,4-DNT. The inset demonstrates the quenching relationship at low concentrations of 2,4-DNT.

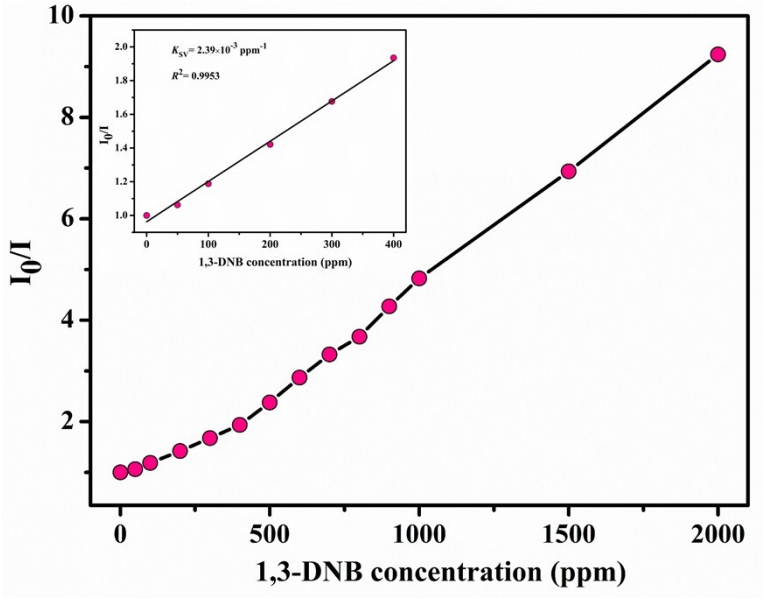

Figure S23. SV curve for **1** by gradual addition of 1,3-DNB. The inset demonstrates the quenching relationship at low concentrations of 1,3-DNB.

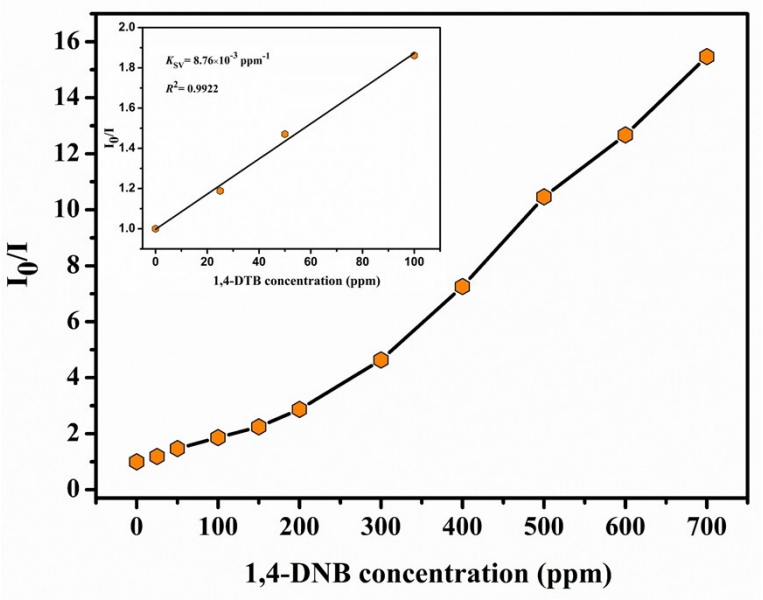

Figure S24. SV curve for **1** by gradual addition of 1,4-DNB. The inset demonstrates the quenching relationship at low concentrations of 1,4-DNB.

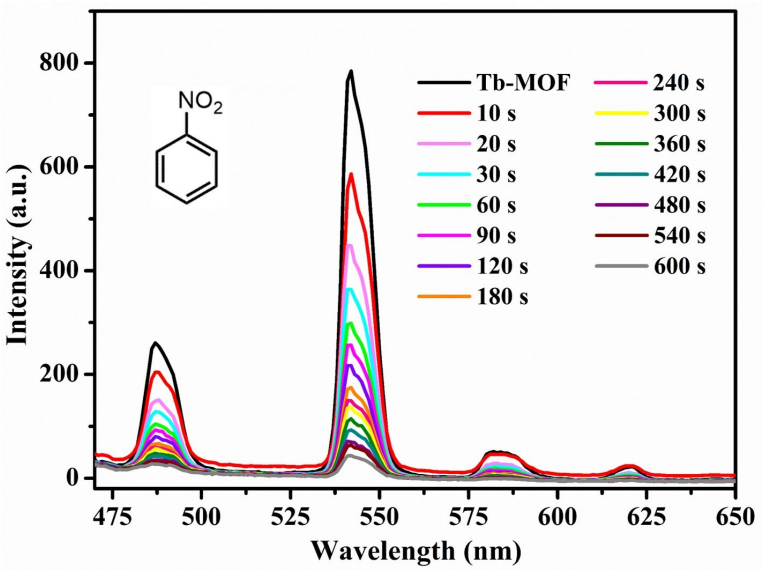

Figure S25. The time-dependent emission spectra of the **1** in NB vapor.

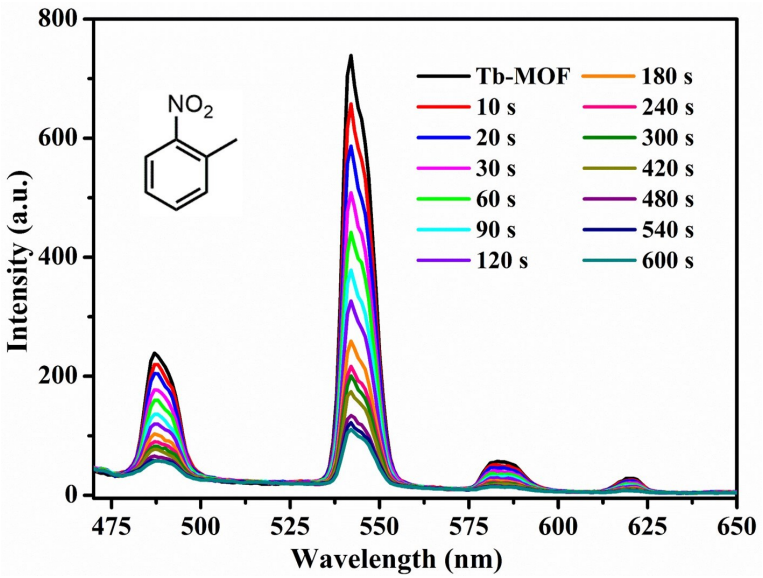

Figure S26. The time-dependent emission spectra of the **1** in 2-NT vapor.

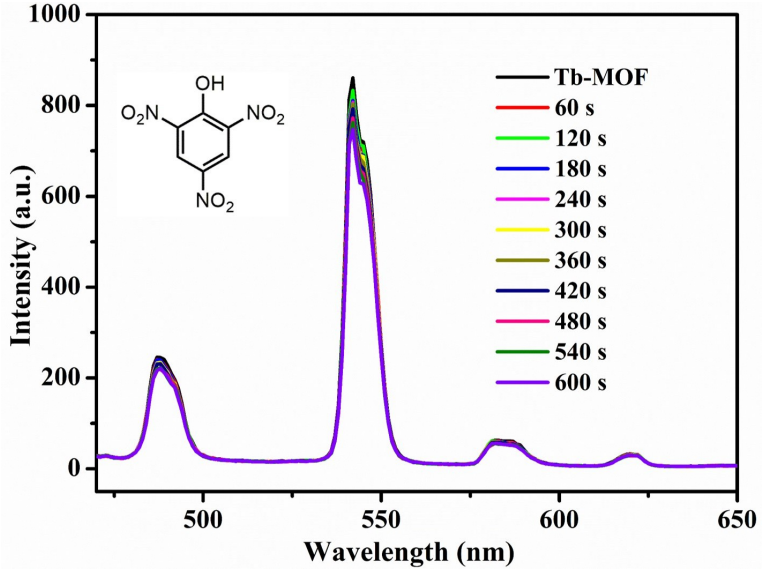

Figure S27. The time-dependent emission spectra of the **1** in TNP vapor.

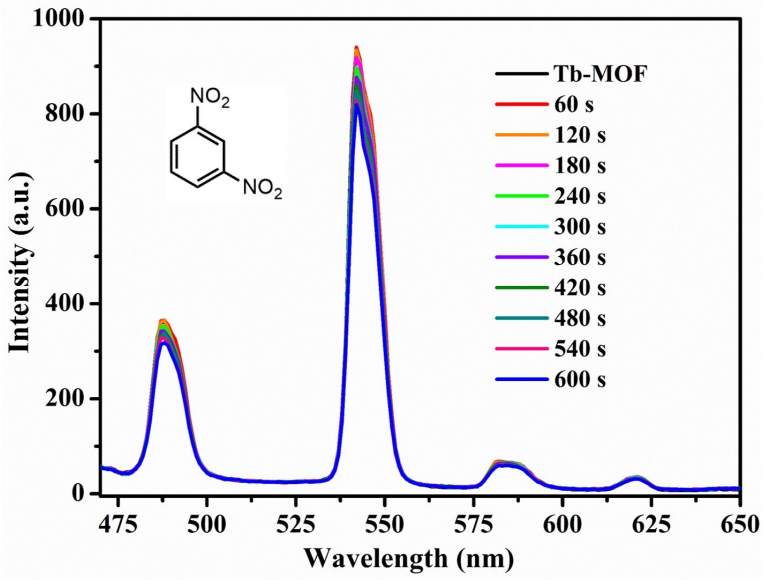

Figure S28. The time-dependent emission spectra of the **1** in 1,3-DNB vapor.

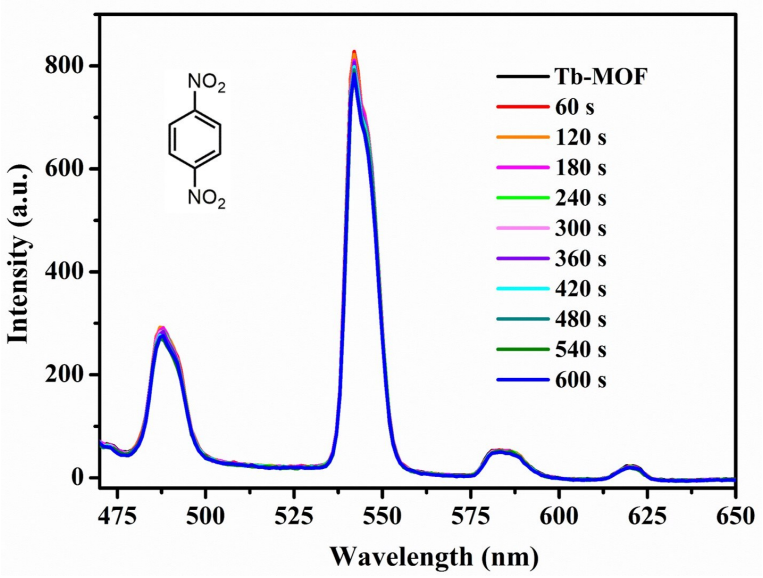

Figure S29. The time-dependent emission spectra of the **1** in 1,4-DNB vapor.

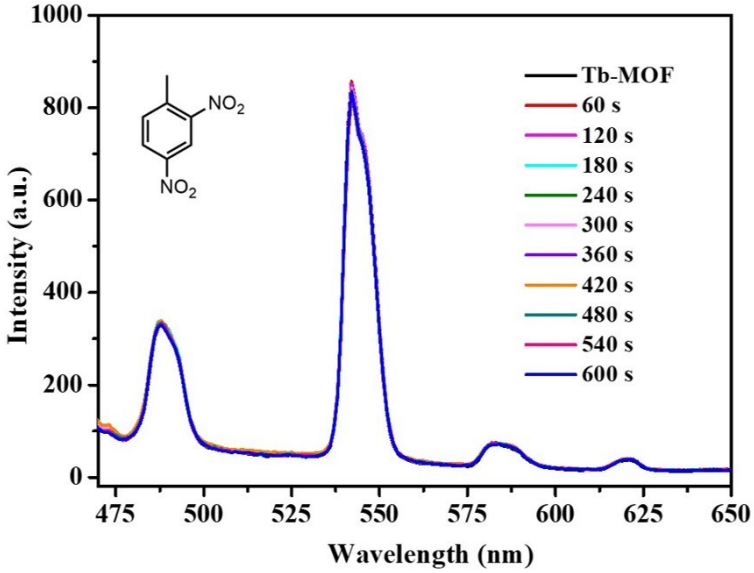

Figure S30. The time-dependent emission spectra of the **1** in 2,4-DNT vapor.

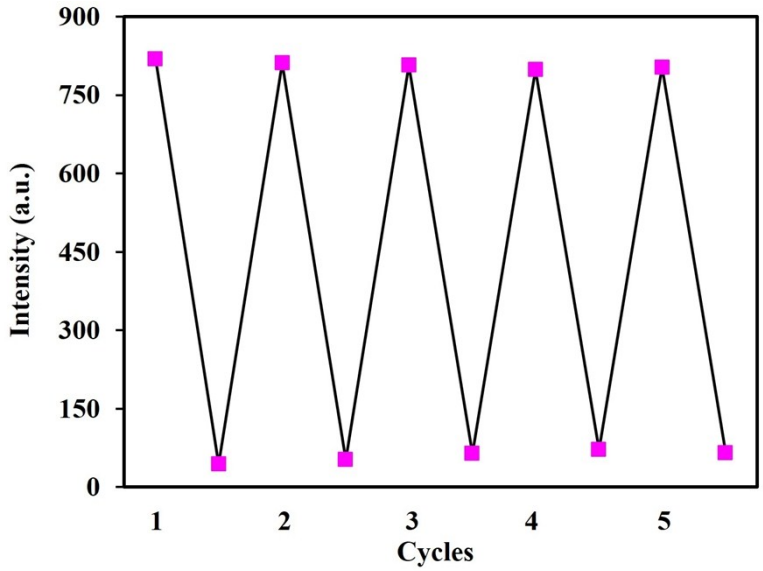

Figure S31. The quenching and recovery tests of **1** in NB vapor.

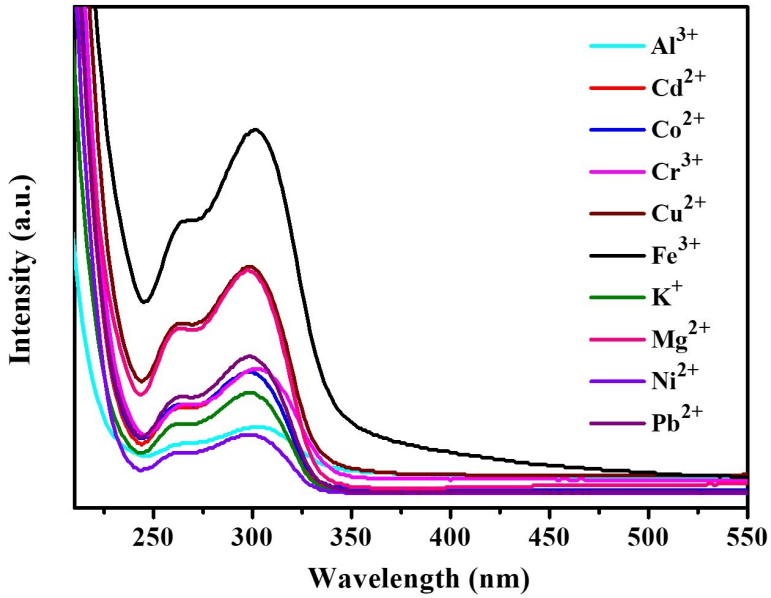

Figure S32. The UV-vis absorption spectrum of $M(NO_3)_X$ aqueous solutions.

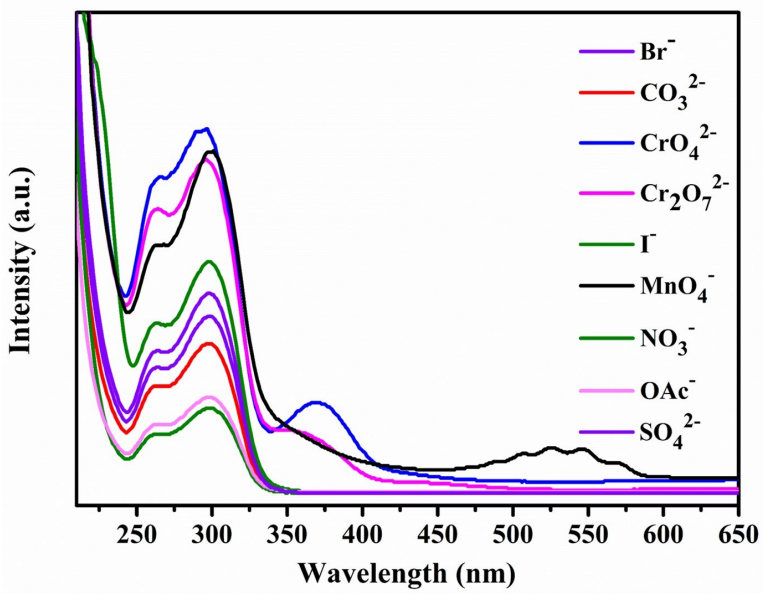

Figure S33. The UV-vis absorption spectrum of $K(anion)_x$ aqueous solutions.

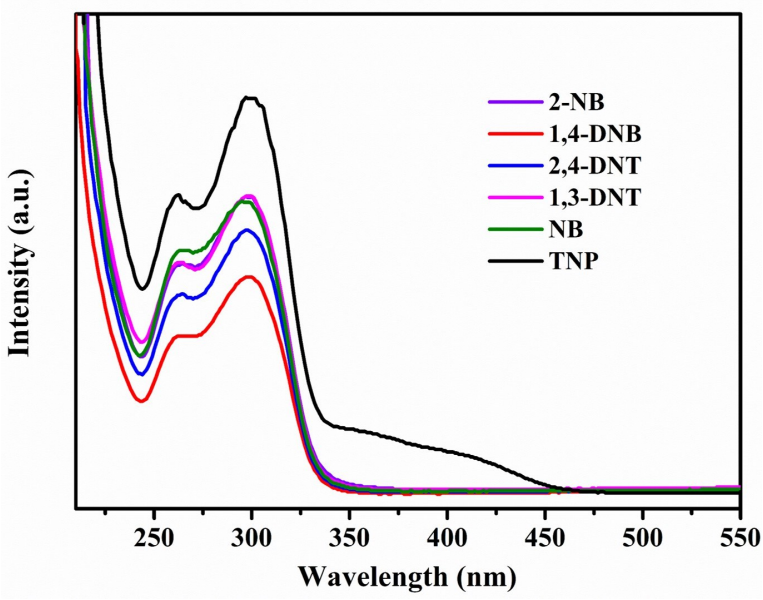

Figure S34. The UV-vis absorption spectrum of the selected NACs in water.

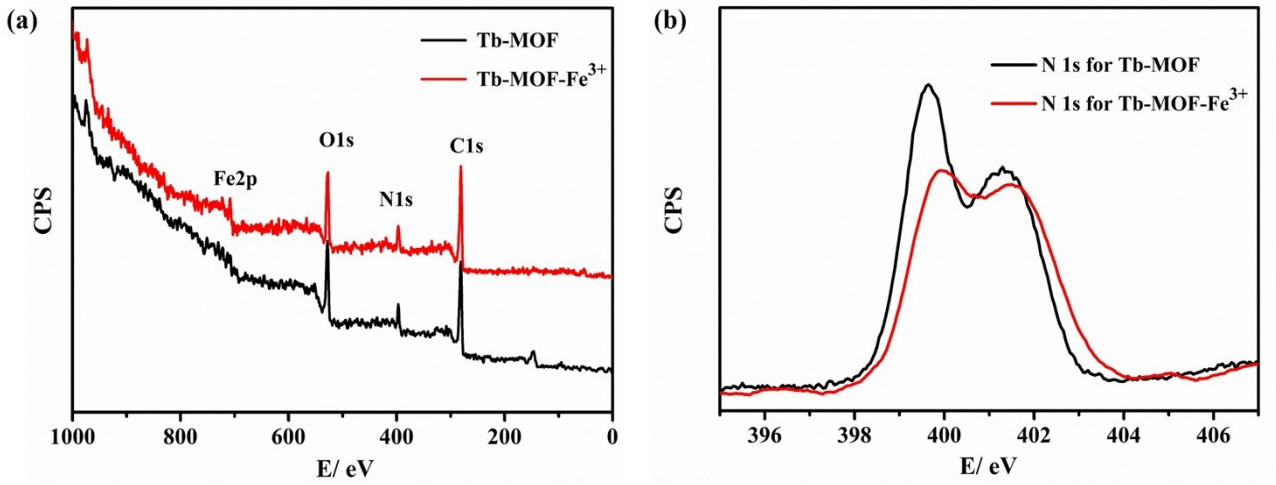

Figure S35. XPS spectra of **1** and Fe^{3+}-**1** (a) and N 1s for **1** and Fe^{3+}-**1** (b).

Table S4. A comparison of selected luminescent MOFs for the detection of Fe^{3+} ion, MnO_4^- anion and TNP solution.

substrates	MOF	Detection limit/(mol/L)	K_{SV} (M^{-1})	Ref.
Fe^{3+}	$[(CH_3)_2NH_2]\cdot[Tb(bptc)]\cdot$xsolvents	10^{-5}	—	S8
Fe^{3+}	$[Tb_4(OH)_4(DSOA)_2(H_2O)_8]\cdot(H_2O)_8$	10^{-6}	3543	9b
Fe^{3+}	$[Eu(HL)(H_2O)_2]\cdot 2H_2O$	10^{-6}	—	9c
Fe^{3+}	EuL	10^{-4}	—	9d

Fe^{3+}	$[Eu(BTPCA)(H_2O)]\cdot 2DMF\cdot 3H_2O$	10^{-5}	—	S9
Fe^{3+}	$[Eu(HL_2)(DMF)(H_2O)_2](H2O)_3$	10^{-5}	1.52×10^{3}	S10
Fe^{3+}	$[Tb(HL_2)(DMF)(H_2O)_2](H_2O)_3$	10^{-5}	4.48×10^{3}	S10
Fe^{3+}	$\{[Eu(L)\ (BPDC)_{1/2}(NO_3)]\cdot H_2O\}_n$	5.0×10^{-7}	5.16×10^{4}	S11
Fe^{3+}	$([Eu_2(L_4)_3(DMA)(H_2O)_3](DMA)(H_2O)_{4.5}$	—	1.07×10^{4}	S12
Fe^{3+}	$[Tb(TBOT)(H_2O)](H_2O)_4(DMF)(NMP)_{0.5}$	1.3×10^{-4}	5.51×10^{3}	S13
MnO_4^-	$[Tb(TBOT)(H_2O)](H_2O)_4(DMF)(NMP)_{0.5}$	3.4×10^{-4}	6.63×10^{4}	S13
MnO_4^-	$[Ba_3La_{0.5}(\mu_3\text{-}L_8)_{2.5}(H_2O)_3(DMF)](DMF)_3$	2.8×10^{-7}	7.73×10^{3}	S14
TNP	[{Eu-CP}	—	9642	S9
TNP	$[Tb(L)(OH)]\cdot x(solv)$	—	1.75×10^{4}	13c
TNP	$[Zn_2(TPOM)(NH_2\text{–}BDC)_2]\cdot 4H_2O$	9.8×10^{-7}	4.6×10^{4}	S15
TNP	$[NH_2(CH_3)_2][Zn_4O(bpt)_2(bdc\text{-}NH_2)_{0.5}]\cdot 5DMF$	5.6×10^{-7}	6.19×10^{4}	S16
TNP	$[Zn_2(H_2L)_2(Bpy)_2(H_2O)_3\cdot H_2O]$	4.9×10^{-7}	1.36×10^{4}	S17
TNP	$UiO\text{-}68@NH_2$	1.8×10^{-6}	5.8×10^{4}	S18
TNP	$[Eu_2(MFDA)_2(HCOO)_2(H_2O)_6]\cdot(H_2O)_n$	4.5×10^{-7}	—	S19
TNP	$\{[Zn_2(AIP)_2(azobpe)_2]\cdot(DMF)\cdot(H_2O)\}_n$	6.7×10^{-6}	3.11×10^{4}	S20
Fe^{3+}	**Compound 1**	**4.8×10^{-7}**	**1.88×10^{4}**	**this work**
$MnO4^-$	**Compound 1**	**1.7×10^{-7}**	**5.18×10^{4}**	**this work**
TNP	**Compound 1**	**3.0×10^{-7}**	**3.43×10^{4}**	**this work**

References

(1) N. N. Mao, P. Hu, F. Yu, X. Chen, G. L. Zhuang, T. L. Zhang and B. Li, *CrystEngComm*, 2017, **19**, 4587.

(2) O. V. Dolomanov, L. J. Bourhis, R. J. Gildea, J. A. K. Howard, H. Puschmann, *J. Appl. Cryst.,* 2009, **42**, 339.

(3) A. L. Spek, *J. Appl. Cryst.,* 2003, **36**, 7.

(4) J. S. Yang and T. M. Swager, *J. Am. Chem. Soc.,* 1998, **120**, 11864.

(5) R. Hoffmann, *J. Chem. Phys.,* 1963, **39**, 1397.

(6) A. J. Lan, K. H. Li, H. H. Wu, L. Z. Kong, N. Nijem, D. H. Olson, T. J. Emge, Y.

J. Chabal, D. C. Langreth, M. C. Hong and J. Li, *Inorg. Chem.,* 2009, **48**, 7165.

(7) J. C. Sanchez and W. C. Trogler, *J. Mater. Chem.,* 2008, **18**, 3143.

(8) X. L. Zhao, D. Tian, Q. Gao, H. W. Sun, J. Xu and X. H. Bu, *Dalton Trans.,* 2016, **45**, 1040.

(9) Q. Tang, S. X. Liu, Y. Liu, J. Miao, S. J. Li, L. Zhang, Z. Shi and Z. P. Zheng, *Inorg. Chem.,* 2013, **52**, 2799.

(10) S. T. Zhang, J. Yang, H. Wu, Y. Y. Liu and J. F. Ma, *Chem. - Eur. J.,* 2015, **21**, 15806.

(11) W. Yan, C. L. Zhang, S. G. Chen, L. J. Han and H. G. Zheng, *ACS Appl. Mater. Interfaces,* 2017, **9**, 1629.

(12) L. Li, Q. Chen, Z. Niu, X. Zhou, T. Yang and W. Huang, *J. Mater. Chem. C,* 2016, **4**, 1900.

(13) M. Chen, W. M. Xu, J. Y. Tian, H. Cui, J. X. Zhang, C. S. Liu and M. Du, *J. Mater. Chem. C,* 2017, **5**, 2015.

(14) B. Ding, S. X. Liu, Y. Cheng, C. Guo, X. X. Wu, J. H. Guo, Y. Y. Liu and Y. Li, *Inorg. Chem.,* 2016, **55**, 4391.

(15) S. S. Dhankhar, N. Sharma, S. Kumar, T. J. D. Kumar and C. M. Nagaraja, *Chem. - Eur. J.,* 2017, **23**, 16204.

(16) S. Xing, Q. Bing, Q. Hui, J. Liu, T. Bai, G. Li, Z. Shi, S. Feng and R. Xu, *ACS Appl. Mater. Interfaces*, 2017, **9**, 23828.

(17) A. Buragohain, M. Yousufuddin, M. Sarma and S. Biswas, *Cryst. Growth Des.,* 2016, **16**, 842.

(18) S. S. Nagarkar, A. V. Desai, P. Samanta and S. K. Ghosh, *Dalton Trans.,* 2015, **44**, 15175.

(19) X. H. Zhou, L. Li, H. H. Li, A. Li, T. Yang and W. Huang, *Dalton Trans.,* 2013, **42**, 12403.

(20) Y. Deng, N. Chen, Q. Li, X. Wu, X. Huang, Z. Lin and Y. Zhao, *Cryst. Growth Des*., 2017, **17**, 3170.